2.C A Time-Resolving, Conically Curved Crystal Spectrograph for Laser-Plasma Studies

Analysis of x-ray line emission has long been used in measuring temperature and density in high-temperature plasmas, both astrophysical and laboratory produced. The emission lines produced, their precise wavelengths and spectral shape, and their relative intensities all provide information on detailed plasma conditions.[1] For laser-produced plasmas, the plasma conditions strongly reflect processes of absorption of laser energy, heat, and compression of the material: x-ray analysis helps elucidate the physics of each process. Among laboratory plasmas, laser-produced plasmas stand out in their ultrashort (nanosecond to picosecond) time behavior and in the extremes of high densities and temperatures produced. These conditions make laser plasmas important tools for extending our theoretical understanding and modeling of transient ionizations and atomic-state physics.[2] Such studies are of particular value to current investigations of x-ray laser schemes.[3]

To pursue these issues with laser plasmas requires spectrographs capable of providing good time resolution (< 50 ps) with at least moderate spectral resolving power ($\lambda/\Delta\lambda \gtrsim 500$). Currently, the combination of a Bragg crystal spectrograph and an x-ray streak camera, recording an x-ray spectrum dispersed in time,[4] is the best answer to these needs. Such devices are capable of less than 20-ps time resolution, and spectral resolving power $\lambda/\Delta\lambda$ greater than 1000.

In addition to good temporal and spectral resolution, the design of some experiments requires large quantum collection and efficiency. An example of such a need is in studies in which thin layers or small amounts of specific materials are embedded in the shell or fuel to provide an x-ray emission signature at some stage in the interaction process. In such studies, the perturbation induced by the signature material on its host should be minimized, and so the amount of material, and its emitted radiation, is designed to be minimal. The detection of weak x-ray signals, with high time and spectral resolution, poses special problems in laser-fusion experiments. One approach to increasing collection efficiency has been to locate the camera closer to the plasma. Given the steadily increasing energy of multikilojoule laser systems used in fusion-related studies, and the hostile magnetic and plasma environment near a target, there is much interest in changes that permit streak spectrographs to be located further from the target, while still more efficiently recording the x-ray emission.

Image intensifiers exposing photographic film already have efficiencies adequate to record single electrons incident on the phosphor of the streak camera's image converter tube, and so the objective must be to increase the photoelectron signal. One avenue has been the search for different photocathode materials of higher x-ray quantum-conversion efficiency.[5] Another approach has been to change the design of the image converter tube through the introduction of an electron-optic astigmatism that permits the use of a wider streak slit by condensing the width of the slit to a line, while still imaging along the slit length;[6] in this

way, the slit subtends a large solid angle without compromising the time-resolution contribution determined by the ultimate width of the streak slit imaged at the phosphor.[7] Third has been the development of spectrographs of moderate resolution that intercept and focus a greater solid angle of radiation.

The most notable of such collecting crystal spectrographs is the Von Hamos cylindrical spectrograph.[8] In this design, a curved crystal defines a cylinder whose axis passes through the radiation source point. Owing to the cylindrical symmetry, all rays of a given wavelength emanating from the source point reconverge on this same axis (where photographic film is positioned) after Bragg reflection at the cylindrical crystal. For an extended source, most points lie some small distance from the cylinder axis, resulting in imperfect convergence; in practice, focused intensities 100 times those of planar crystal spectrographs are reached.[9,10]

This spectrograph design is somewhat inconvenient for use in conjunction with x-ray streak cameras, since the spectral focus is along a radial axis, whereas image converter tubes are most conveniently and commonly used with photocathodes normal to this axis. The use of a Von Hamos spectrograph with a streak camera in this orientation results in effective collection of only a very narrow spectral range in the region near the intersection of the Von Hamos and photocathode axes,[11] since the Von Hamos focusing degrades quickly for points removed from its axis. In the true Von Hamos configuration, the need to orient the image converter tube perpendicular to a radius from the target generally requires that the streak camera be situated completely outside the principal vacuum chamber.[12] For laser-fusion target chambers this added distance, and the fixed Von Hamos geometry, typically results in awkwardly large dispersions.

Designs permitting spectra to be focused in a line perpendicular to the radius from the target include crystals bent to the figure of a section of a cone,[13] and to the figure of a section of a torus.[14] The latter configuration demonstrates 50 times the brightness of a comparably deployed flat crystal, while imaging the target at the same time. Here we describe the experimental implementation of a conically bent crystal spectrograph originally described by T. A. Hall,[13] using a Muscovite mica crystal bent to a cone figure of 23.1° half-angle. The spectrograph, when coupled to an x-ray streak camera, time-resolves He-like lines and Li-like satellites useful in determining the density and temperature of thin layers (0.05 μm–0.1 μm) of Al and Ti, isolated in spherical CH targets, during irradiation by the 24-beam, 351-nm OMEGA laser system. Examples of the data produced by a preliminary version of the spectrograph are drawn from some of these experiments.

The conical-crystal spectrometer has been proposed[13] as a modification of the Von Hamos design [Fig. 26.13(a)] for focusing a spectrum along a line perpendicular to the radius from the target, rather than along it. This is accomplished by curving the spectrometer crystal to a section of the surface of a cone oriented as shown in Fig. 26.13(b). In this configuration, the cone has its apex lying in the recording plane

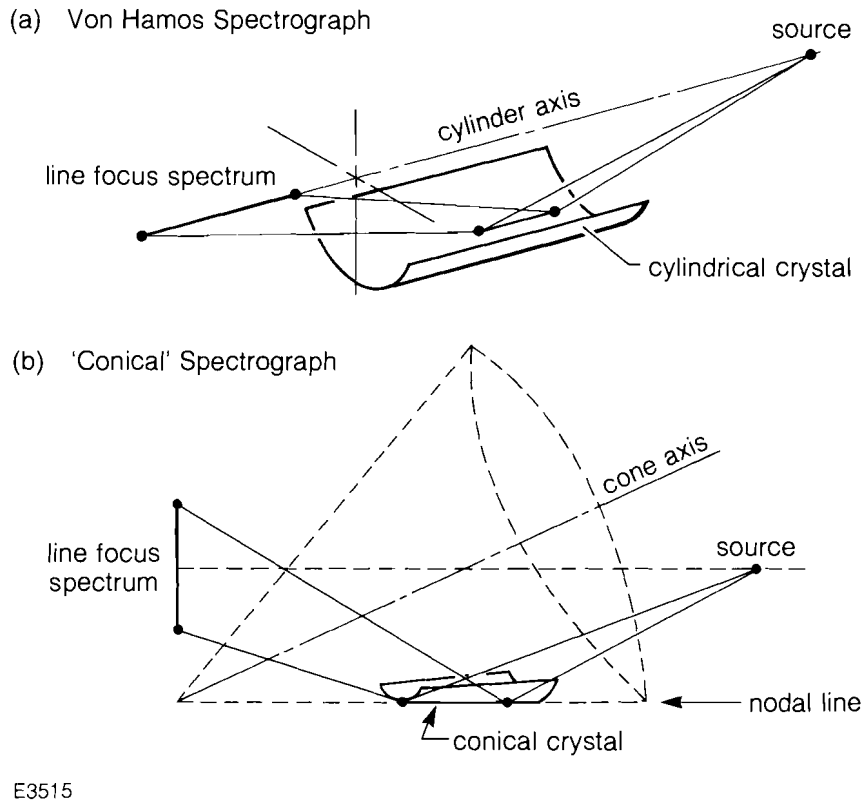

Fig. 26.13
Comparison of (a) Von Hamos and (b) conical x-ray-collecting crystal spectrograph designs. The conically bent crystal spectrograph produces a spectrum focused in a line perpendicular to the line of sight to target.

(lying perpendicular to a radius from the source), its cone axis crossing this radius at the midpoint, and its nodal line parallel to the radius. This crystal curving is a simple sheet bending (bent in one direction only) and is suitable for a wide range of crystals and radii.

In projecting the spectrum into a line perpendicular to the radius axis, two advantages of the Von Hamos design are necessarily lost. In the Von Hamos geometry, source and image are nominally equidistant from the point of reflection at the crystal. As a result of this symmetry, the spread of wavelengths due to the mosaic structure of the crystal survives only in second order (mosaic focusing).[10,15] Consequently, mosaic crystals, which generally have high integrated reflectivity, can be used without disadvantage in resolution. For spectrographs that form a perpendicular spectrum, this symmetry and the benefits of mosaic focusing are lost,[16] except perhaps for a very small region of the image near the source radius.

For the ideal case of a single-point source, the focusing of an ideal Von Hamos spectrograph is perfect, and all rays of a given wavelength obviously take the same transit time to their image point, a concern to time-resolving applications. That ideal case is impossible to recreate in a perpendicular-spectrum spectrograph; even a single-point source

cannot be made to image perfectly with all rays arriving simultaneously.[17] The conical spectrograph, and others like it, therefore depend on detailed analysis, usually ray tracing, to evaluate their temporal, spatial, and spectral characteristics.

With such ray tracing for a conical spectrograph, Hall[13] has shown quantitatively that, as the width of the cone surface used increases, the size of a point source's aberrated image increases in the imaging direction, i.e., perpendicular to the line focus. Along the spectral axis, the image size increases more slowly with increasing crystal width, and then decreases to an optimal value before again increasing monotonically. Hall also calculated the resolving power that results from this spectral confusion, convolved with the intrinsic limits of the crystal, and derived its dependence on wavelength about the best-imaged point. Using a 45° cone angle, and 0.02 as the ratio of (crystal width)/(image-plane distance), he found that for a roughly $\pm 10\%$ wavelength range about the optimal wavelength the resolution of the spectrograph is limited by the crystal, rather than the geometry.[18] Also, he calculated the focused intensity of the spectral image; over a large range of incident Bragg angles, this calculated brightness is more than 1000 times the brightness obtained from a planar spectrograph of similar specifications.

In combination with an x-ray streak camera, the brightness improvement is somewhat less than this figure. Once the image of the source lies completely within the limits of the streak camera slit aperture, there is no further gain in brightness in the streaked image as spectrograph focus is improved. Instead, for conventional electron-optic designs in which the slit aperture is imaged across its width, the streak slit image at the phosphor is narrowed, and the contribution of the writing speed and slit width to the overall time-resolution limit is reduced. In the device described here, a 1-mm slit width is used at the photocathode to facilitate alignment of the spectrograph. The width of the line focus, imaged at the phosphor, thus determines the writing-rate time-resolution limit.

Implementation

Crystal support mounts for the LLE spectrograph were fabricated on a conventional precision lathe, turning a frustum of a hollow cone of 23.1° cone half angle (Fig. 26.14). The narrow end of the frustum had an inside diameter of 19.25 cm, the base, one of 26.80 cm. The inner surface of the frustum was figured as the crystal-bearing surface and was machined to about $\pm$ 25-μm tolerance with slow variation over a scale of about 5 mm. On a smaller scale, the surface roughness was absorbed in gluing the crystal. Before the piece was removed from the lathe, a series of scores was cut, by a tool bit, into the outside surface of the frustum to provide an accurate alignment reference of the cone's nodal lines. Later, the piece was sectioned into a number of mounts 3.8 cm $\times$ 9.5 cm by cutting along every other scored line. The mounts were aligned in a jig, using the nodal lines, to affix attachment rings.

Mica (Muscovite) crystals were mounted on these substrates. They had been designed so that the Bragg condition ($n\lambda = 2d \sin\theta$) would be satisfied for He-like resonance emission ($1s^2$–$1s2p$: $^1S_0$–$^1P_1$) from Al

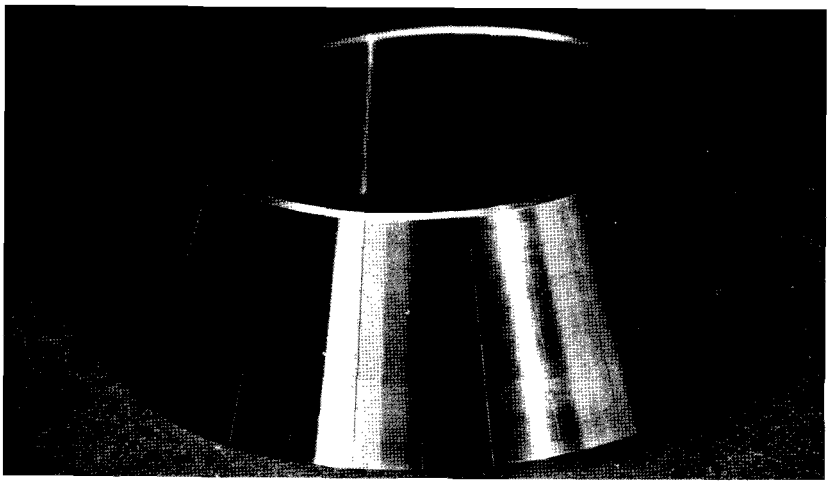

E3968

Fig. 26.14
Photograph of section of a cone, lathe-turned in aluminum, from which several mounts for spectrograph crystals were cut.

(λ = 7.757 Å; in first order) and Ti (λ = 2.62 Å; in third order) near the optimum point of the crystal midway between source and photocathode. The overall wavelength range dispersed at the photocathode was 7.5 Å < n λ < 8.1 Å in nth-order Bragg diffraction. Two different crystal attachments were investigated: vacuum mounting, using a low-viscosity cyanoacrylate glue to hold the crystal permanently, after it was drawn down onto the mount by evacuating through several tiny holes in the substrate; and pressing the crystal into a layer of epoxy.

The mounted crystal was attached to the streak camera as shown in Fig. 26.15. Critical to the spectrograph setup is the precise positioning of the apex of the spectrograph cone in the plane of the photocathode,

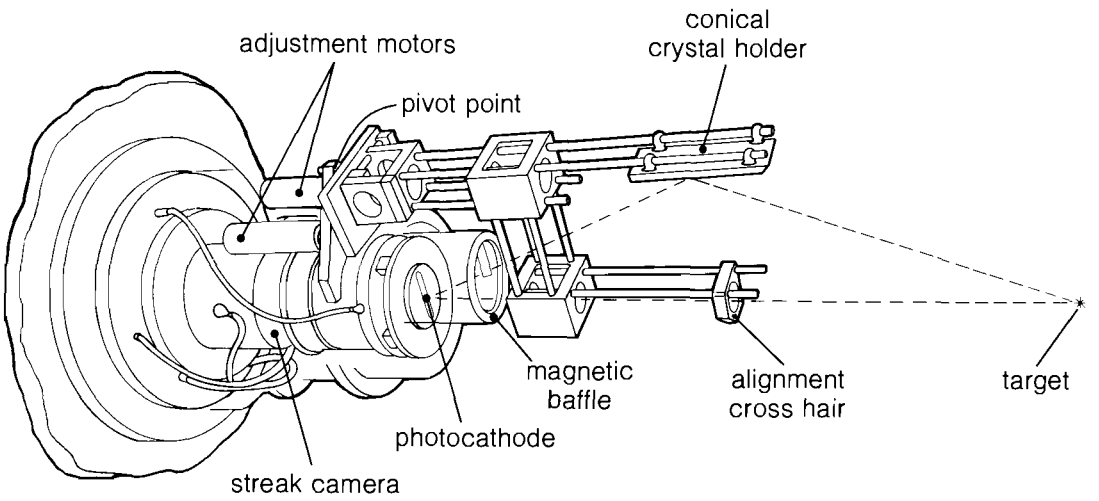

E3409

Fig. 26.15
Configuration of the conical streak spectrometer. The crystal holder is positioned in its mount in such a way that the apex of the cone to which it belongs coincides with the pivot point of the mount. Remotely controlled adjustment motors then align the crystal to the target.

along the axis of the photocathode slit. This is accomplished by supporting the crystal mount on a frame that pivots on a spherical bearing centered on that position. Then the crystal mount is set in the frame, with the nodal line passing through that point. Part of this frame rests on two linear actuators oriented 90° apart relative to the pivot. This permits the spectrograph to be aligned to the target remotely in vacuum, while remaining aligned to the streak camera.

To align to the target, a cross hair was mounted above the spectrograph at the same distance calculated for the height of the photocathode center above the cone apex. In use, then, a telescope installed opposite the device was aligned to the axis between target and the center of the photocathode, and the structure was remotely driven to place the cross hair on this axis. This procedure ensured that the spectrograph was oriented with its cone nodal line parallel to the target-photocathode axis, and at the correct distance. In use, there was little difficulty in aligning the spectrograph to the 1-mm streak slit.

The streak spectrograph was a modified RCA 73435 design,[19] deployed re-entrant to the target chamber and evacuated along with it to a pressure of 5×10^{-6} Torr. The target-to-photocathode distance was 57 cm, producing a dispersion of about 19 mÅ/mm at the photocathode. The streak camera itself was capable of a spatial resolution of roughly 10 ℓp/mm, and overmatched the spectral resolution expected for the spectrograph. This overmatching was to improve quantitative data reduction, particularly that of line shapes.

Experimental Results

The conical streak spectrograph was used in recording x-ray emission from targets irradiated with the OMEGA 24-beam UV (351-nm) laser system. Parylene (CH)-coated spherical targets were used in which a spherical, 0.05-μm- to 0.1-μm-thick layer of Ti or Al was located at a depth of 1.5 μm–2.5 μm (Fig. 26.16). In addition, data were taken for

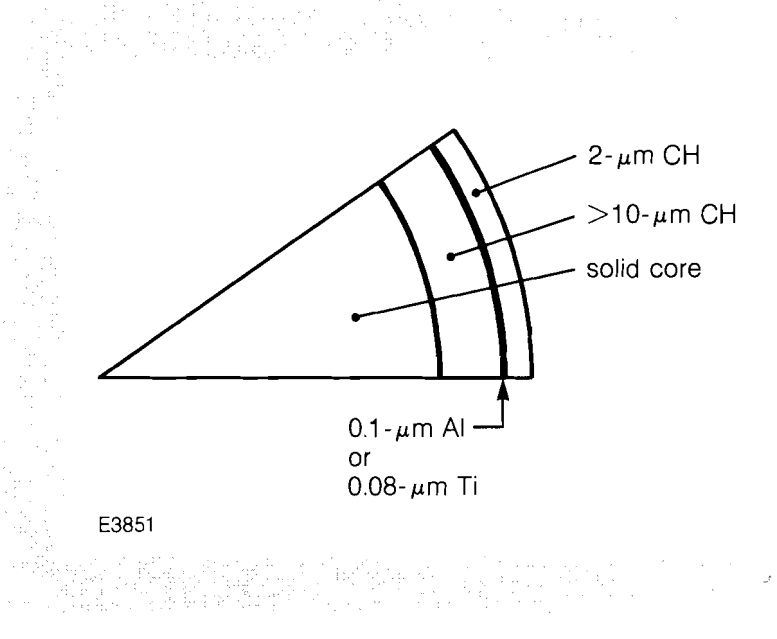

Fig. 26.16
Schematic drawing of the thin-layer targets used. Thin layers of aluminum or titanium were located within plastic targets, to produce x-ray emission characteristic of plasma conditions at that depth.

several DT-filled microballoons to which Kr had been added as a diagnostic emitter. All targets were uniformly irradiated at a peak intensity of 4×10^{14} W/cm^2, and He-like spectra as well as Li-like satellites of the metallic layers, or emission from Si and Kr, were time resolved.

A comparison of spectra, taken with the streak spectrograph, of thick (2-μm) and thin (0.1-μm) Al layers is shown in Fig. 26.17. For this figure the film response characteristics are already removed, but no account of the reflectivity of the mica for different wavelengths is taken. Mica shows strong features in its spectral reflectivity over this range. In this case, the thick Al was bare, and the thin layer was buried at a depth of about 2 μm. Without additional attenuation, the intensity from the thicker Al layer was excessive and, during the streak, produced severe photoelectron-current pinching in the imperfect vacuum of the tube.

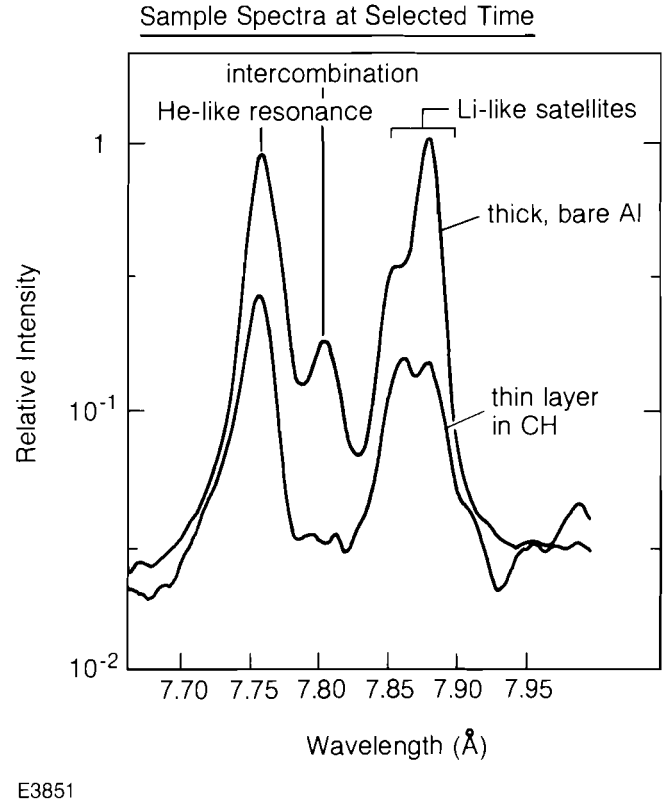

Fig. 26.17
Comparison of spectra taken at early time in the emission from a thick (2-μm) bare aluminum target, and from a thin-layer target of the type in Fig. 26.16. The times at which each spectrum was taken are not the same with respect to the laser pulse.

Similar spectra from a thin, embedded Ti layer are displayed in Fig. 26.18(a). Time traces made of each line feature can be seen in Fig. 26.18(b). Ratios of these lines help in determining the temperature and density[20] evolution of the emitting region, which, for sufficiently thin layers, is well localized.

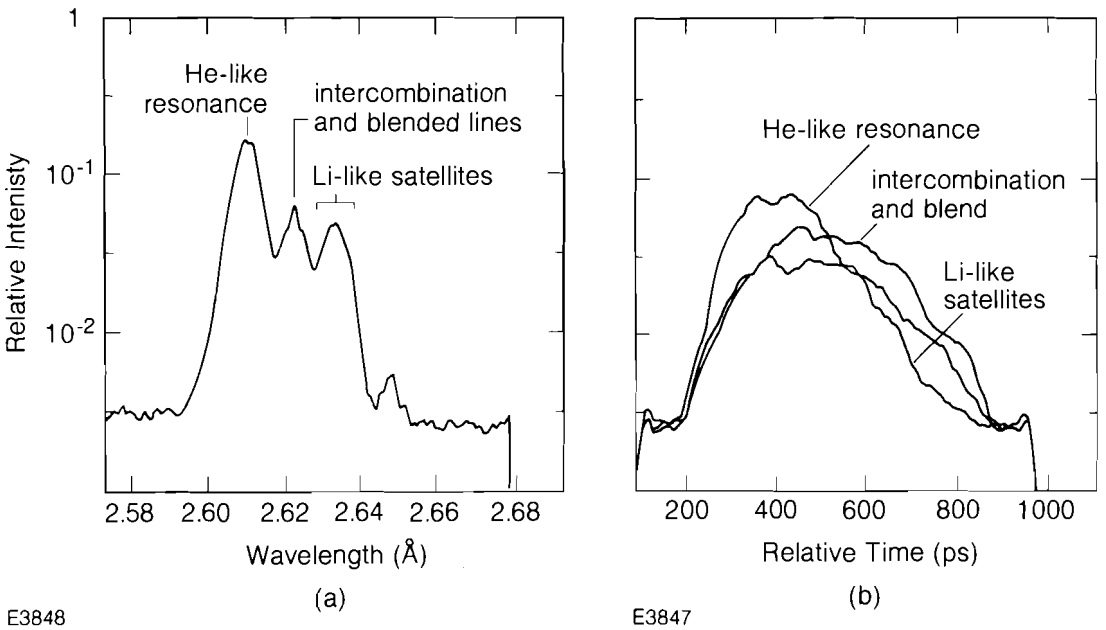

Fig. 26.18
Sample spectrum (a), produced at a selected time, from a titanium thin-layer target of the type shown in Fig. 26.16. Part (b) shows the history of emission of several spectral features during the laser pulse.

Figure 26.19(a) shows a perspective plot of the emission dynamics during the implosion of a Kr/DT-filled glass microballoon. A sample spectrum at a selected time is shown in Fig. 26.19(b).

Conclusions

The streak spectrometer produced by combining a conically bent crystal spectrograph with an x-ray streak camera provided an effective device for time-resolving low-flux spectra from laser-produced plasmas. The intensity improvement over a similarly deployed planar-crystal spectrograph should be equal to the ratio of widths at the crystal that subtend the streak slit; this indicates a collected-flux increase of a factor of 50–100, consistent with observation.

The time resolution of the current system is limited by the effective width of the streak-slit image at the phosphor and is estimated at 40 ps. With characterization of a better-focused spectrum, or with an astigmatic electron-optic design, this figure can be lowered to 10–20 ps. The spectral resolving power of the time-resolving system is estimated at $\lambda/\Delta\lambda \sim 600$, currently limited by the quality of the figure of the crystal mount. This is highlighted by data taken with crystals that had been vacuum mounted: vacuum mounting produced excellent conformation to the substrate, and in data taken with such mounts, very small periodic machining irregularities produced substantial structure in the spectra.

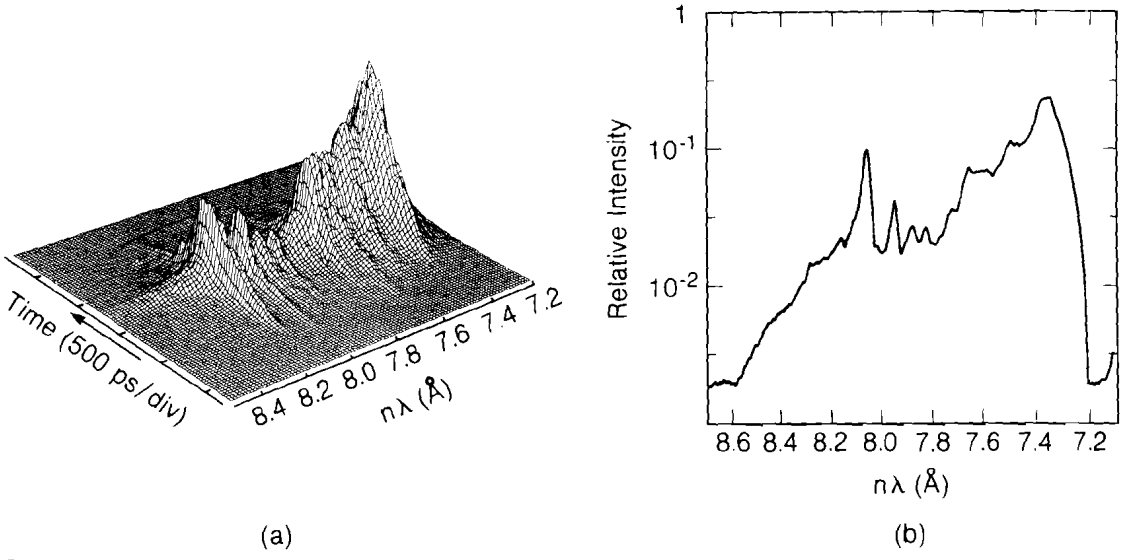

Fig. 26.19
Perspective plot (a) of the temporally and spectrally resolved emission from an imploding deuterium- and tritium-filled microballoon target, to which a small amount of krypton gas was added. A sample spectrum, taken at a time near the peak of emission, is shown in (b).

Recently, high-quality diamond-turned mounts have been prepared. Mica, used in third order, has been retained for studies of Ti He-like resonance, and, in second order, for Ar-filled microballoon implosions. The large degree of structure in the first-order spectral reflectivity of mica in the region of interest makes it inappropriate for studying Al emission around 7.8 Å. Mica has been replaced by KAP mounted on a 17.05° half-angle cone. With these changes implemented, it is anticipated that the resolution of the spectrograph will be limited either by source size, for studies using thin emitting layers embedded in 200-μm- to 300-μm-diameter CH spheres, or by the intrinsic limits of the crystal, as in implosion studies of filled microballoons. We expect to test these improvements in the near future.

ACKNOWLEDGMENT

This work was supported by the U.S. Department of Energy Office of Inertial Fusion under agreement No. DE-FC08-85DP40200 and by the Laser Fusion Feasibility Project at the Laboratory for Laser Energetics, which has the following sponsors: Empire State Electric Energy Research Corporation, General Electric Company, New York State Energy Research and Development Authority, Ontario Hydro, Southern California Edison Company, and the University of Rochester. Such support does not imply endorsement of the content by any of the above parties.

Muscovite sheets of large size were kindly provided by Dr. Barry Luther-Davies of the Australian National University, Department of Engineering Physics.

REFERENCES

1. Good general references to the use of x-ray spectroscopy in plasma diagnosis include: M. H. Key and R. J. Hutcheon, *Adv. At. Mol. Phys.* **16**, 201 (1980); C. DeMichelis and M. Mattioli, *Nucl. Fusion* **21**, 677 (1981).
2. See, for example: S. R. Stone and J. C. Weisheit, LLNL Report UCID-20262 (1984).
3. M. D. Rosen *et al., Phys. Rev. Lett.* **54**, 106 (1985); D. L. Matthews *et al., ibid.* **54**, 110 (1985); J. F. Seely, C. M. Brown, U. Feldman, M. Richardson, B. Yaakobi, and W. E. Behring, *Opt. Commun.* **54**, 289 (1985). For a general review of the short-wavelength laser approach, see R. W. Waynant and R. C. Elton, *Proc. IEEE* **64**, 1058 (1976); F. V. Bunkin, V. I. Derzhiev, and S. I. Yakovlenko, *Kvant. Elektron. (Moscow)* **8**, 1621 (1981) [*Sov. J. Quantum Electron.* **11**, 981 (1981)].
4. For description of streak spectrometers, see, for example: LLE Review **14**, 16 (1983); M. H. Key *et al., Phys. Rev. Lett.* **44**, 1669 (1980).
5. See, for example: B. L. Henke, J. P. Knauer, and K. Premaratne, *J. Appl. Phys.* **52**, 1509 (1981).
6. P. A. Jaanimagi and B. L. Henke (to be published).
7. G. I. Brukhnevitch, V. K. Cevokin, Yu. S. Kasyanov, V. V. Korobkin, A. A. Malyutin, A. M. Prokhorov, M. C. Richardson, M. Ya. Schelev, and B. M. Stepanov, *Phys. Lett.* **51A**, 249 (1975).
8. L. Von Hamos, *Z. Kristallogr.* **101**, 17 (1939); C. B. Van Den Berg and H. Brinkman, *Physica* **21**, 85 (1955).
9. B. Yaakobi, R. E. Turner, H. W. Schnopper, and P. O. Taylor, *Rev. Sci. Instrum.* **50**, 1609 (1979).
10. B. Yaakobi and V. Bhajavatula, LLE Report No. 89 (1979).
11. B. J. MacGowan, in Annual Report to the Laser Facility Committee, Rutherford Appleton Report RL-82-039, 1.28–1.30 (1982).
12. N. H. Burnett *et al., Phys. Rev. A* **29**, 2294 (1984).
13. T. A. Hall, *J. Phys. E* **17**, 110 (1984).
14. A. Hauer, J. D. Kilkenny, and O. L. Landen, *Rev. Sci. Instrum.* **56**, 803 (1985); P. Kirkpatrick and A. V. Baez, *J. Opt. Soc. Am.* **33**, 766 (1948).
15. B. Yaakobi and A. J. Burek, *IEEE J. Quantum Electron.* **QE-19**, 1841 (1983).
16. It is not possible to construct a collecting-crystal spectrograph with an image axis perpendicular to the radius to the target and still retain the geometry for mosaic focusing found in the Von Hamos design.
17. R. S. Marjoribanks and M. C. Richardson (to be published).

18. For cones of smaller angle, it might be expected that this performance would be improved.

19. P. A. Jaanimagi and M. C. Richardson, *Rev. Sci. Instrum.* **27**, 1095 (1983).

20. V. A. Boiko, S. A. Pikuz, and A. Ya. Faenov, *J. Phys. B* **12**, 1889 (1979); E. V. Aglitskii, V. A. Boiko, A. V. Vinogradov, and E. A. Yukov, *Sov. J. Quantum Electron.* **4**, 322 (1974); see also reference 1.